Cellulose (2022) 29:6283–6299
https://doi.org/10.1007/s10570-022-04654-y

ORIGINAL RESEARCH

Dirhodium complex immobilization on modified cellulose for highly selective heterogeneous cyclopropanation reactions

Lorenz Rösler · Mark V. Höfler · Hergen Breitzke · Till Wissel · Kevin Herr · Henrike Heise · Torsten Gutmann · Gerd Buntkowsky

Received: 12 February 2022 / Accepted: 16 May 2022 / Published online: 11 June 2022

Abstract A novel, efficient approach for the functionalization of microcrystalline cellulose (MCC) is presented. The as-obtained material allows the immobilization of chiral dirhodium catalysts preserving their enantioselectivity in asymmetric cyclopropanation reactions. As model, microcrystalline cellulose is modified with a polyethylene glycol derived linker, and Rh_2(*S*-DOSP)$_4$ is grafted on the material to produce a heterogeneous catalyst. SEM images at different stages of the immobilization show an unchanging uniform morphology, providing constantly good separation characteristics. The modification of the cellulose material with the polyethylene derived linker and the immobilization process are monitored using DNP enhanced $^{1}H \rightarrow {}^{13}C$ CP MAS NMR, quantitative ^{19}F MAS NMR, TGA and ICP-OES analysis, confirming the success of the immobilization as well as the stability of bonds between the used linker molecule and the cellulose material. Finally, the evaluation of the produced catalyst is demonstrated in the asymmetric cyclopropanation reaction between styrene and methyl(*E*)-2-diazo-4-phenylbut-3-enoate showing excellent enantioselectivity with an ee of nearly 90% over a wide temperature range as well as good recyclability characteristics in four consecutive catalysis cycles.

Keywords Immobilization · Asymmetric cyclopropanation · Dirhodium · NMR spectroscopy · Dynamic nuclear polarization

Supplementary Information The online version contains supplementary material available at https://doi.org/10.1007/s10570-022-04654-y.

L. Rösler · M. V. Höfler · H. Breitzke · T. Wissel · K. Herr · T. Gutmann (✉) · G. Buntkowsky (✉)
Institute of Inorganic and Physical Chemistry, Technical University of Darmstadt, Alarich-Weiss-Straße 8, 64287 Darmstadt, Germany
e-mail: gutmann@chemie.tu-darmstadt.de

G. Buntkowsky
e-mail: gerd.buntkowsky@chemie.tu-darmstadt.de

H. Heise
Institute of Biological Information Processing, Structural Biochemistry (IBI-7) and Jülich Center for Structural Biology (JuStruct), Forschungszentrum Jülich, 52425 Jülich, Germany

H. Heise
Institut Für Physikalische Biologie, Heinrich-Heine-Universität Düsseldorf, 40225 Düsseldorf, Germany

Introduction

Dirhodium(II) complexes such as tetrakis[(*S*)-(-)-*N*-(p-dodecylphenylsulfonyl)prolinato]dirhodium(II) (Rh_2(*S*-DOSP)$_4$) are well established as catalysts in many processes, making them indispensable in producing pharmaceuticals and fine chemicals (Chen et al. 2017; Boruta et al. 2012; DeAngelis et al. 2009; El-Deftar et al. 2012; Gadakh et al. 2015; Gutmann et al. 2015; Li and Davies 2010; Liu et al. 2015;

Rackl et al. 2017). The versatility of dirhodium(II) catalysts includes C–H, C–O, C–N, and C–C bond as well as ylide formations, X–H insertions, carbene-type reactions like cyclopropanations and many more (Adly et al. 2016; Davies and Denton 2009; Davies and Manning 2008; Davies and Morton 2011; Doyle et al. 2010; Huang et al. 2019; Miyazawa et al. 2016; Reddy et al. 2006; Roizen et al. 2012; Zhu et al. 2016). A protruding aspect in dirhodium catalyst research is enantioselective synthesis (Davies and Walji 2003; El-Deftar et al. 2012; Li and Davies 2010; Natori et al. 2015; Panne et al. 2008; Vos et al. 2002; Doyle et al. 2010; Miyazawa et al. 2016). The importance of this topic arises mainly from the biological activity of enantiomerically pure substances, especially in drug production (Williams and Lee 1985; Takeda et al. 2010; Li et al. 2020). To highlight one of the many uses of enantioselective dirhodium catalysis, metal catalyzed asymmetric carbenoid cyclopropanation is an example of great scientific interest (Sun et al. 2002, Singh and DattaGupta 1997, Maas 2004, Li et al. 2021a, Li et al. 2020, Doyle et al. 1990, Davies and Pelphrey 2011, Davies and Morton 2011, Davies and Antoulinakis 2001, Bianchini and Lee 2000, Awata and Arai 2012, Anciaux et al. 1980, Adly et al. 2016). The products of many asymmetric cyclopropanation reactions, namely polysubstituted cyclopropane derivatives, are widely used as drugs, such as the antidepressant Milnacipran (Doyle and Hu 2001; Bonnaud et al. 1987). In most of these reactions, homogeneous catalysts are used due to their high activity and enantioselectivity. These catalysts, however, pose disadvantages, especially concerning catalyst separation and recovery (Corma and Garcia 2006; Liu et al. 2017; Zhao et al. 2006). The separation is essential in the production of pharmaceuticals since remaining toxic heavy metals like rhodium may contaminate the product. Next, the high cost of rhodium is a compelling argument towards the simplification of the recovery procedure.

A possible solution to overcome these issues is the immobilization of homogeneous dirhodium catalysts on insoluble support materials, which is the focus of many research groups (Adly and Ghanem 2016; Davies and Walji 2005; Davies et al. 2004; Dikarev et al. 2010; Doyle et al. 2002, 2003; Hultman et al. 2003; Liu et al. 2018; Oohara et al. 2012; Sun et al. 2002; Takeda et al. 2010, 2011; Trindade et al. 2012). They have presented approaches for immobilizing dirhodium catalysts on mesoporous silica (Li et al. 2021a; Liu et al. 2017; Gutmann et al. 2015) or on crystalline nanocellulose (Liu et al. 2015). Here, the solid support replaces costly separation steps by simple filtration or centrifugation after the reaction. Recently, dirhodium complexes have also been heterogenized as metal–organic coordination-polymers as shown by Kaskel and co-workers (Nickerl et al. 2014) and some of the authors who prepared achiral as well as chiral coordination-polymers (Li et al. 2020, 2021b; Liu et al. 2016, 2018). Although, these results have demonstrated the feasibility to immobilize achiral and chiral dirhodium catalysts, there is still potential for improvement. The immobilization on inorganic supports like SBA-15, while showing good enantioselectivities, poses the problem of recovery of the precious metal after deactivation of the catalyst, since the silica material cannot easily be removed from the catalyst, i.e., harsh conditions like strong acids and microwave irradiation or hydrofluoric acid have to be applied to recover the precious metals. The immobilization as a metal–organic coordination-polymer necessitates the use of high amounts of rhodium, making this approach rather expensive. A solution to overcome both of these drawbacks is the immobilization of homogeneous, enantioselective catalysts on organic supports like polystyrene (Davies and Walji 2003; Takeda et al. 2010). Organic support materials can easily be burned after deactivation of the catalyst and the synthesis of the immobilized catalysts requires lower amounts of the active metal compared to the synthesis of metal–organic coordination polymers. A further environmentally friendly improvement to the use of supports such as polystyrene or other synthetic polymers is the use of naturally occurring biopolymers such as cellulose, chitin or chitosan. For example, cellulose can be easily obtained, is stable as a solid in a wide variety of solvents and reaction conditions and carries accessible functional groups on the surface, making it an excellent material as catalyst support (Chauhan and Yan 2015; Eberhardt et al. 2001; Keshipour et al. 2013; Li et al. 2018; Seyednejhad et al. 2019; Yamada et al. 2020; Yasukawa et al. 2015; Liu et al. 2015). The synthesis of modified biopolymers by a grafting-type modification compared to monomer modification with subsequent polymerization offers the advantage of simple preparation pathways due to the easy separation of the heterogeneous reaction products from reactants.

In these works, exclusively achiral catalysts are used. To the best of our knowledge, for rhodium only one example has been published so far, where a cellulose supported catalyst was employed in enantioselective synthesis (Yasukawa et al. 2020). Their proposed approach however used a cellulose-based rhodium nanoparticle catalyst and chiral, homogeneous auxiliaries to obtain selectivity. While this is an advance compared to the use of neat homogeneous catalysts, the synthesis and especially the separation and recycling of the homogeneous auxiliaries still necessitate additional reprocessing after each catalytic cycle. Thus, there is a great demand to synthesize highly enantioselective, immobilized catalysts on cellulose materials as well as to monitor the immobilization steps using a combination of established and advanced analytical techniques.

In this work, we present a synthesis strategy for novel biopolymer supported enantioselective catalysts by immobilization of chiral dirhodium catalysts on cellulose. The approach is based on the attachment of a long-chain, pyridine-based linker molecule (TTDS-Nic) to microcrystalline cellulose. The functionalized biopolymer is then used to immobilize the homogeneous Rh_2(*S*-DOSP)$_4$ catalyst. The synthesis steps are monitored by means of thermogravimetric analysis (TGA), scanning electron microscopy (SEM), and liquid nuclear magnetic resonance spectroscopy (NMR) as well as liquid chromatography (LC). Furthermore, dynamic nuclear polarization enhanced solid-state NMR (solid-state DNP) is used as a powerful technique to investigate structural changes at the nanoscale during the functionalization of the cellulose materials. This technique uses the three-order of magnitude higher polarization of electron spins, typically from an external source such as from stable binitroxyl radicals, and transfer it into nuclear spin polarization (see recent reviews and references therein (Rankin et al. 2019; Lilly Thankamony et al. 2017; Gutmann et al. 2019)). This allows to drastically enhance sensitivity in solid state NMR experiments and enables the detection of small amounts of surface functionalization and insensitive nuclei in natural abundance on cellulose-based materials as it has been impressively demonstrated by some recent works (Berruyer et al. 2021; Höfler et al. 2021; Groszewicz et al. 2020; Gutmann et al. 2017; Zhao et al. 2014; Perras et al. 2017; Takahashi et al. 2012). This **cel-cat** is then applied in catalytic activity tests to monitor the enantioselectivity employing the intermolecular cyclopropanation reaction between styrene and methyl (3*E*)-2-diazo-4-phenyl-3-butenoate (**4**) as model reaction. Finally, the reusability and leaching properties of the **cel-cat** are inspected to validate the stability and sustainability of the novel catalyst system.

Experimental

Materials

All purchased materials were used without further purification unless specified otherwise. Pentane, ammonium chloride, THF, toluene, piperidine, ethanol, 1-ethyl-3-(3-dimethylaminopropyl)carbodiimide hydrochloride (EDC•HCl), DMF, 4-dimethyl-aminopyridine (DMAP), magnesium sulfate, hydrochloric acid, sodium bicarbonate and *N*,*N*-diisopropylethylamine (DIPEA) were purchased from Carl Roth GmbH + Co. KG. Styrene, diethyl ether, 1,8-diazabicyclo[5.4.0]undec-7-ene (DBU), 4-acetamidobenzenesulfonyl azide (p-ABSA), methyl (3*E*)-4-phenyl-3-butenoate, 3-fluoro-4-pyridinecarboxylic acid, isonicotinic acid, methylene chloride, microcrystalline cellulose, ethyl acetate and 4,7,10-trioxa-1,13-tridecanediamine (TTD) as well as deuterated solvents for NMR analyses were purchased from Sigma-Aldrich. Rh_2(*S*-DOSP)$_4$ was purchased from Strem Chemicals, Inc., succinic anhydride from Acros Organics, acetonitrile (MeCN) and water for HPLC analyses from VWR and *N*-(9-fluorenylmethoxycarbonyloxy)succinimide (Fmoc-OSu) from abcr GmbH & Co KG.

Characterization

^{1}H- and ^{13}C-NMR spectra in liquid phase were recorded at room temperature by the analytical department of the Technical University of Darmstadt using a Bruker DRX Avance spectrometer. The ^{1}H spectra were recorded at a frequency of 500.13 MHz, ^{13}C spectra at a frequency of 125.77 MHz, respectively, employing single pulse excitation. The chemical shift is given in ppm using the signals of the solvent as secondary reference to TMS in $CDCl_3$ ($\delta = 0$ ppm).

$^{1}H \rightarrow {}^{13}C$ CP MAS DNP measurements were performed on a Bruker Avance III HD 600 MHz DNP spectrometer at 14.1 T leading to a frequency of 600.00 MHz for ^{1}H and 150.87 MHz for ^{13}C. The spectrometer is equipped with a triple resonance $^{1}H/X/Y$ low temperature MAS probe operating at 100 K using the maximum cooling power. This spectrometer is connected to a high-power, high frequency gyrotron system producing continuous microwaves with a frequency of 395 GHz. The samples were prepared by incipient wetness impregnation according to ref. (Sauvée et al. 2013) using a 15 mM AMUPol solution in DMSO-d_6/D_2O/H_2O (60/30/10). Thereby, 15 mg of the sample were impregnated with 15 µL of this solution. The spectra were measured using 1024 scans and a recycle delay of $1.3 \bullet T_B$ where T_B is the build-up time obtainable from a ^{1}H saturation recovery experiment of the sample, measured with microwave irradiation. The contact time was set to 2.5 ms and a linear ramp from 100 to 50 was used to efficiently transfer ^{1}H spin polarization to ^{13}C under MAS conditions. The acquisition time was set to 10 ms and spinal64 (Fung et al. 2000) proton decoupling was applied during data acquisition. The spectra were recorded at 10.5 kHz spinning frequency and referenced to a silicon plug inside the rotor (0 ppm).

^{19}F MAS NMR measurements were performed on a Bruker Avance II + 400 MHz spectrometer at 9.4 T corresponding to a frequency of 376.48 MHz for ^{19}F. The spectrometer is equipped with a 3.2 mm HF/X/Y MAS NMR resonance probe. The spectra were measured using a one pulse sequence with 908 scans and a recycle delay of 300 s to ensure to be quantitative. The acquisition time was set to 82 ms and a π/9 pulse with a length of 0.46 µs was used. Details of the quantification using BaF_2 are given in the ESI.

The High-Performance Liquid Chromatograms were recorded using a Waters Alliance e2695 HPLC System equipped with a Waters 2998 Photodiode Array Detector and a Reprosil Chiral OM-R 5µ 250 × 4.6 mm column or a ISAspher 100–3 C18 50 × 4.6 mm column, depending on the analyte. As eluents, mixtures of water and MeCN with 0.1% of trifluoracetic acid as additive were used in different gradients.

The mass spectrometric analyses were performed on an Impact II mass spectrometer from Bruker Daltonic, with a qTOF analyzer using either ESI or APCI as methods for ionization.

Thermogravimetric analyses were performed on a Netzsch TG 209 F3 Tarsus®. After drying the sample under nitrogen flow (40 mL/min) at 120 °C for 1 h to remove solvents, the sample was heated with a rate of 15 K/min to a temperature of 950 °C holding that temperature for 30 min. The measured weight differentials were corrected with a blank measurement.

SEM images were recorded on a XL30-FEG electron microscope from Philips. The images were recorded with an acceleration voltage of 15 kV and a spot size of 3. The magnification of all images was set to 12 000 to achieve comparable results. The samples were all coated with a gold coating using a sputter coater in an argon atmosphere.

UV/Vis spectra were acquired on a TIDAS S 500 MCS UV/NIR spectrometer of J&M Analytik AG with quartz cuvettes of 10 mm width. All samples were measured against a dark scan and a reference scan employing the solvent without analyte. The absorbance was measured in single scan mode with an integration time of 30 ms and 200 accumulations.

Determination of the degree of functionalization (DF) of mod-cel-1

The degree of functionalization (DF) of Fmoc-TTDS-Cellulose (**mod-cel-1**) was determined by UV-spectroscopic analysis of the concentration of the dibenzofulvene-piperidine adduct formed in the deprotection step of **mod-cel-1**. 20 mg of Fmoc-TTDS-Cellulose were suspended in 5 mL of a 20% (v/v) solution of piperidine in DMF. After ultrasonication for 5 min, the suspension was filtered and topped up through the used filter to 20 mL with the piperidine solution to rinse out remaining dibenzolfulvene-piperidine adduct. The absorption of the resulting solution was then measured at 301 nm and the concentration calculated using an external standard (see supporting information Figure S8).

Synthesis of Fmoc-TTDS (3)

N-Fmoc-*N*′-succinyl-4,7,10-trioxa-1,13-tridecanediamine (Fig. 1) was synthesized based on the procedure in the literature (Zhao et al. 1999). 5.00 g (1.00 eq.) of succinic anhydride dissolved in 200 mL MeCN were added dropwise to a stirred solution of 11.02 g (1.00 eq.) of TTD in 200 mL MeCN at 0 °C over the course of 1 h. The solution

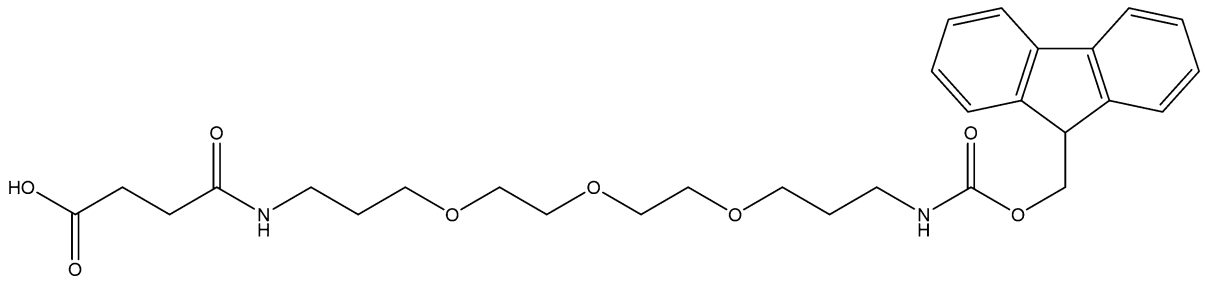

1-(9*H*-fluoren-9-yl)-3,19-dioxo-2,8,11,14-tetraoxa-4,18-diazadocosan-22-oic acid
Fmoc-TTDS
3

Fig. 1 Molecular structure of Fmoc-TTDS (**3**)

was then decanted from the precipitating intermediate *N*-succinyl-4,7,10-trioxa-1,13-tridecanediamine, which was then dissolved in 500 mL of a mixture of Water and MeCN (50/50, v/v). To this solution, 21.93 g (1.30 eq.) of FmocOSu in 250 mL of MeCN were added dropwise over the course of 45 min at 0 °C, before adjusting the pH to a value of 8 with DIPEA. The mixture was allowed to warm to room temperature and stirred overnight. After removing the solvent from the mixture under reduced pressure, the resulting crude product was mixed with 500 mL of an aqueous sodium bicarbonate solution. The mixture was then extracted three times with portions of 250 mL ethyl acetate. The aqueous phase was adjusted to a pH of 1 using concentrated hydrochloric acid before extracting it again three times with portions of 250 mL ethyl acetate. After drying of the organic phase over magnesium sulphate and removing the solvent under reduced pressure, 17.3 g of the product (**3**) as a colorless oil were obtained.

Yield: 64%; **^{1}H NMR (500 MHz, CD_2Cl_2)**: δ 7.78 (d, *J* = 7.6 Hz, 2H), 7.62 (d, *J* = 7.6 Hz, 2H), 7.40 (t, *J* = 7.5 Hz, 2H), 7.32 (t, *J* = 7.4 Hz, 3H), 4.38 (d, *J* = 7.0 Hz, 2H), 4.25 (dt, *J* = 23.6, 6.7 Hz, 1H), 3.62–3.47 (m, 6H), 3.31 (q, *J* = 6.1 Hz, 2H), 3.25 (q, J = 6.5 Hz, 2H), 2.62 (dd, *J* = 8.8, 4.6 Hz, 2H), 2.48 (t, *J* = 6.6 Hz, 2H), 1.74 (m, 4H); **^{13}C NMR (126 MHz, CD_2Cl_2)**: δ 175.38, 173.14, 157.05, 144.65, 141.75, 128.11, 127.52, 125.57, 120.39, 70.79, 70.48, 69.61, 66.77, 47.78, 39.33, 38.52, 31.19, 30.47, 30.01, 29.27; **HPLC**: R_t = 13.6 min, > 96% @ 214 nm.

Immobilization of Fmoc-TTDS (3) on cellulose

The synthesis of **mod-cel-1** (Fig. 2) was inspired by a procedure in the literature (Cateto and Ragauskas 2011). 1 g Cellulose (1 eq. primary OH-groups) and 1.13 g (1.5 eq.) DMAP were mixed in 100 mL DMF and homogenized in an ultrasonic bath. After the addition of 2.37 g of EDC•HCl (2 eq.) and a second homogenization step, 7 g Fmoc-TTDS (**3**) (2 eq.)

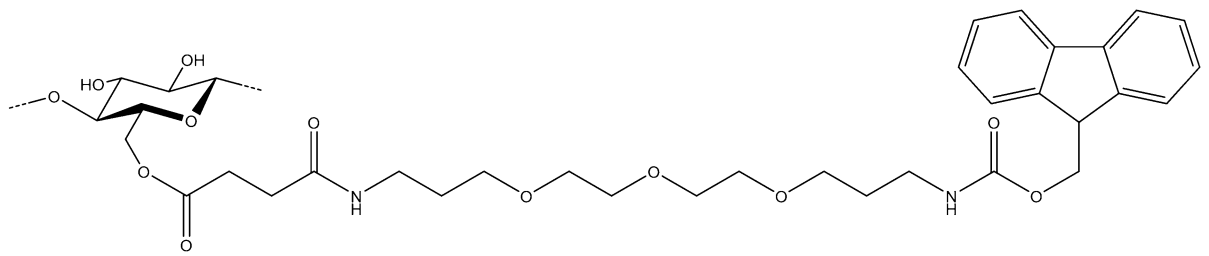

Fmoc-TTDS-Cellulose
mod-cel-1

Fig. 2 Modified monosaccharide fragment of Fmoc-TTDS-Cellulose (**mod-cel-1**)

dissolved in a small amount of DMF were added to the mixture. The mixture was then stirred for 24 h at room temperature before quenching with 10 mL of 2 N hydrochloric acid. The solid was filtered off and washed with 100 mL portions of DMF, ethyl acetate, water, and ethanol before drying it in vacuum yielding 1.06 g of the product (**mod-cel-1**).

Yield (6.8% DF): 87%.

Deprotection of Fmoc-TTDS-cellulose

0.94 g Fmoc-TTDS-Cellulose were shaken briefly in 10 mL of a 20% (v/v) solution of piperidine in DMF. The product was filtered off and washed with 50 mL portions of DMF, methylene chloride, water, ethanol, and ethyl acetate. After drying in vacuum, 0.86 g of the product TTDS-Cellulose (Fig. 3, **mod-cel-2**) were isolated.

Yield (6.8% DF): 94%.

Coupling of (fluorinated) isonicotinic acid to TTDS-cellulose

Analogous to the Steglich-type esterification in the immobilization of Fmoc-TTDS on cellulose the formation of an amide bond between the amino group of the TTDS linker and the nicotinic acid derivative is carried out using EDC•HCl and DMAP. To 0.5 g TTDS-Cellulose (1 eq. amino groups) suspended in 100 mL DMF, 0.57 g DMAP (1.5 eq.) were added. The mixture was homogenized by means of ultrasonication. After the addition of 1.18 g EDC•HCl (2 eq.) and another ultrasonication step, 0.76 g isonicotinic acid (2 eq.) were introduced to the reaction mixture. The reaction was carried out over the course of 24 h at room temperature. The reaction was then quenched using 10 mL of 2 N hydrochloric acid before removing the solvents by filtration. The filter cake was washed with 50 mL portions of DMF, ethyl acetate, water, and ethanol before drying under vacuum. 0.45 g of the product (Fig. 4, **mod-cel-3**) was isolated.

Yield (6.8% DF): 86.7%.

The synthesis of the fluorinated analogue (TTDS-NicF-Cellulose) was carried out in the same way

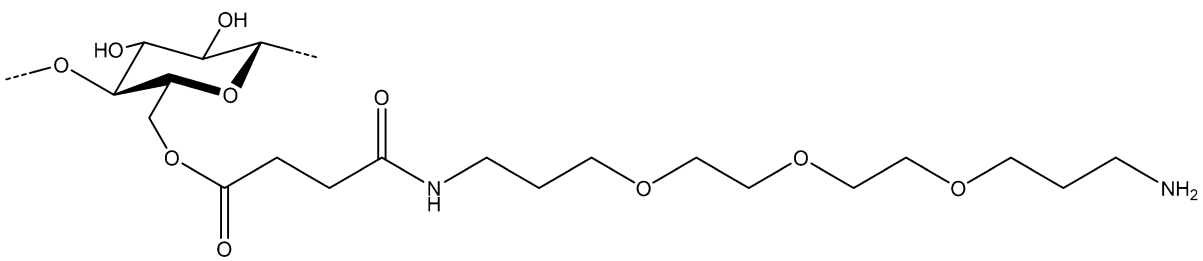

TTDS-Cellulose
mod-cel-2

Fig. 3 Modified monosaccharide fragment of TTDS-Cellulose (**mod-cel-2**)

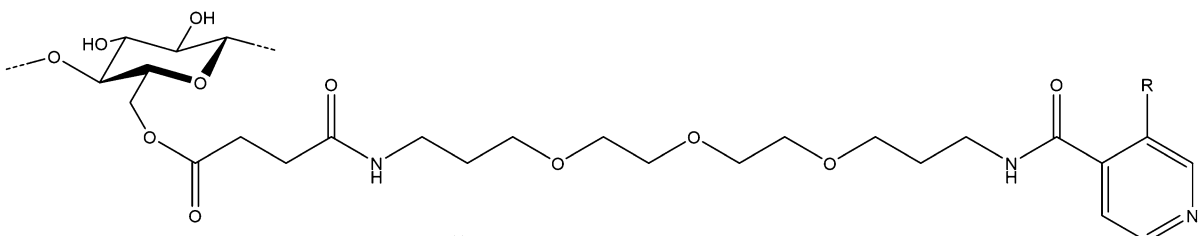

TTDS-Nic[F]-Cellulose
R = H: **mod-cel-3**
R = F: **mod-cel-3a**

Fig. 4 Modified monosaccharide fragment of TTDS-Nic(F)-Cellulose (**mod-cel-3** and **mod-cel-3a**)

using 0.87 g (2 eq.) of 3-fluoro-4-pyridinecarboxylic acid instead of isonicotinic acid. 0.435 g of the product (Fig. 4, **mod-cel-3a**) was isolated.

Yield (6.8% DF): 83.8%.

Immobilization of Rh_2(S-DOSP)$_4$ on mod-cel-3

The immobilization of Rh_2(*S*-DOSP)$_4$ by axial coordination was carried out in 15 mL of degassed toluene under an argon atmosphere. To a suspension of 0.1 g (1 eq.) **mod-cel-3** in toluene, 0.18 g Rh_2(*S*-DOSP)$_4$ were added. The mixture was then gradually heated to 120 °C over the course of 2 h. After 6 h of reflux, the solvent was removed by filtration and the product was washed two times each with 30 mL portions of toluene, THF, and ethanol, resulting in 0.13 g of the product (Fig. 5, **cel-cat**) after drying under vacuum.

Yield (6.8% DF): 77.84%; **ICP-OES**: 4.35 wt.-% Rh.

Synthesis of methyl (3*E*)-2-diazo-4-phenyl-3-butenoate (4)

Methyl (3*E*)-2-diazo-4-phenyl-3-butenoate (Fig. 6) was synthesized according to the procedure described in the literature (Ibbeson et al. 2014). To 2.00 g (1 eq.) methyl (3*E*)-4-phenyl-3-butenoate in 100 mL of dry, degassed MeCN at 0 °C, 4.11 g (1.1 eq.) of 4-acetamidobenzenesulfonyl azide were added under argon atmosphere. After the addition of 3.4 mL (1.1 eq.) of DBU over the course of 15 min, the solution was stirred for additional 3 h at 0 °C under argon atmosphere. The reaction was then quenched adding 50 mL of a concentrated ammonium chloride solution. The resulting mixture was then extracted three times using 50 mL diethyl ether each. The combined organic extracts were then dried over magnesium sulphate before removing the solvents under reduced pressure in an ice bath. The resulting red oil was then purified by column chromatography yielding 2.83 g of the product (**4**) as a red oil.

Yield: 60%; **^{1}H NMR (500 MHz, DMSO):** δ 7.42 (d, J = 7.2 Hz, 2H), 7.31 (t, J = 7.7 Hz, 2H), 7.19 (t, J = 7.1 Hz, 1H), 6.52 (d, J = 16.3 Hz, 1H), 6.48 (d, J = 16.4 Hz, 1H), 3.78 (s, 3H); **^{13}C NMR (126 MHz, DMSO)**: δ 164.82, 136.77, 128.65, 126.93, 111.20, 63.48; **HPLC**: R_t = 17.17 min, > 92% @ 214 nm.

Catalytic asymmetric cyclopropanation

The catalytic cyclopropanation reactions (Scheme 1) were carried out at -78 °C, 0 °C, 10 °C and 35 °C respectively. To a degassed solution of 1.2 M (5 eq.) styrene in 1.10 mL of pentane, 54 mg (1 eq.) methyl (3*E*)-2-diazo-4-phenyl-3-butenoate (**4**) in 2.2 mL pentane were added. 8 mg (0.01 eq.) of the immobilized catalyst (**cel-cat**) were then suspended in the solution and the mixture was stirred for 24 h at the given temperatures above. The reaction mixture was then filtered and analyzed by chiral HPLC using a gradient from 30 to 80% (v/v) of MeCN in water over the course of 25 min with

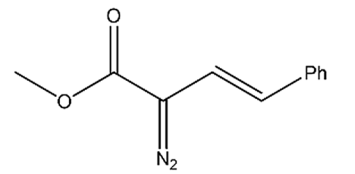

methyl (*E*)-2-diazo-4-phenylbut-3-enoate
4

Fig. 6 Molecular structure of methyl (3E)-2-diazo-4-phenyl-3-butenoate (**4**)

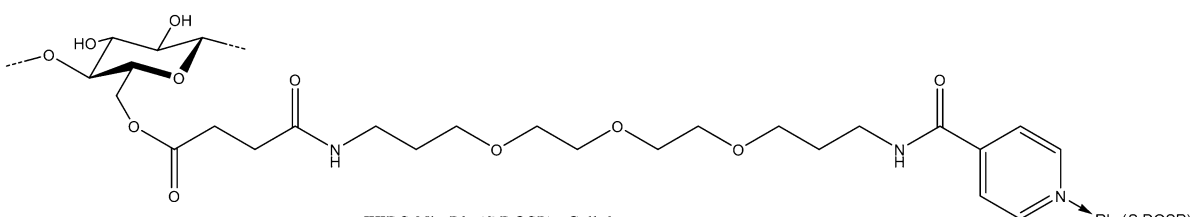

TTDS-Nic-Rh_2(*S*-DOSP)$_4$-Cellulose
cel-cat

Fig. 5 Modified monosaccharide fragment of TTDS-Nic-Rh_2(*S*-DOSP)$_4$-Cellulose (**cel-cat**)

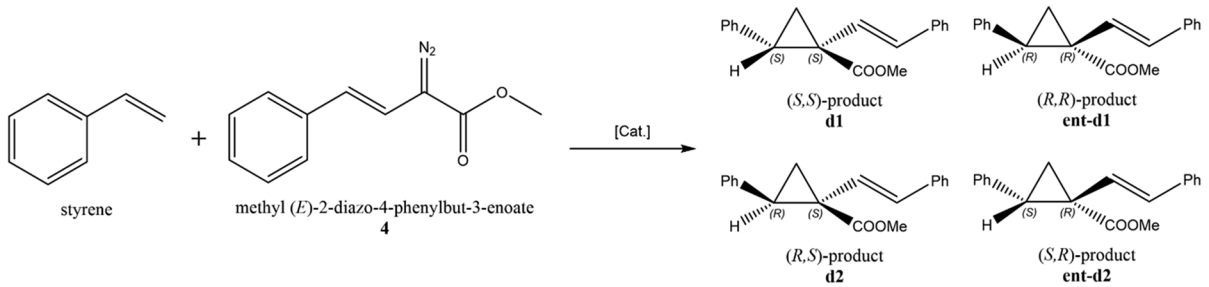

Scheme 1 Catalytic cyclopropanation of methyl (3E)-2-diazo-4-phenyl-3-butenoate (**4**) and styrene

a flow of 1 mL/min employing a Reprosil Chiral OM-R 5µ 250 × 4.6 mm column (see ESI Fig. S9 for an exemplary chromatogram).

To identify the retention times of the enantiomers, the reaction given above was carried out as well with enantiopure homogeneous Rh_2(*S*-DOSP)$_4$ and Rh_2(*R*-DOSP)$_4$ catalysts at − 78 °C.

Recycling of the catalyst

To test the recyclability of the heterogenized catalyst, it was used in the cyclopropanation reaction for 4 consecutive times. For this purpose, 32 mg of the immobilized catalyst were suspended in 5 mL of degassed pentane under an argon atmosphere. To the suspension, 700 µL (5 eq.) styrene were added, and the mixture was heated to 35 °C. To the reaction mixture, a solution of 213 mg of methyl (3*E*)-2-diazo-4-phenyl-3-butenoate (**4**) in 10 mL degassed pentane were added dropwise.

Samples were taken for HPLC analysis directly after the addition of the substrate as well as after each hour in the first 12 h, and then every 12 h to a total reaction time of 48 h.

Results and discussion

Synthesis of the materials

In Scheme 2, the synthesis route for the Fmoc protected linker molecule (**3**) is shown.

This synthesis is based on a Schotten-Baumann type acylation with succinic anhydride on the linear diamine TTD (**1**) without the addition of a base to achieve the single-sided amide TTDS (**2**). After Fmoc-protection of **2**, the isolation of the desired product Fmoc-TTDS (**3**) is readily achieved using the pH-dependent solubility of the linker molecule in comparison with the side products. The protection of the linker molecule is necessary to prevent intramolecular amide formation or dimerization, respectively, during the coupling of the linker to the cellulose. Despite the exclusive stoichiometric control of the reaction to form the mono- instead of the disubstituted diamine, the linker is synthesized with a yield of 64% and a high purity of > 96% (HPLC) without further purification.

As shown in Scheme 3, Fmoc-TTDS-Cellulose (**mod-cel-1**) is then obtained by a Steglich esterification of the linker molecule **3** with the microcrystalline cellulose (**cel**). This step is followed by the

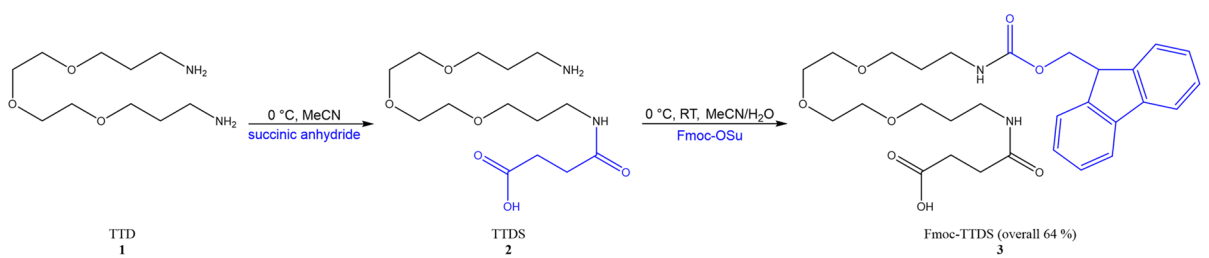

Scheme 2 Synthesis strategy for the linker molecule Fmoc-TTDS (**3**)

deprotection of the amine group to obtain the modified cellulose TTDS-Cellulose (**mod-cel-2**). Finally, the isonicotinic acid derived head group is attached to **mod-cel-2** via an amide bond formation to enable the coordination of the chiral Rh_2(*S*-DOSP)$_4$ catalyst.

For analytical reasons, the isonicotinic acid derived head group is used in two different derivatives: One with a fluorine marker (**mod-cel-3a**) to determine the degree of functionalization via ^{19}F NMR and one without (**mod-cel-3**) for the attachment of Rh_2(*S*-DOSP)$_4$. The attachment of the Rh_2(*S*-DOSP)$_4$ to **mod-cel-3** is then achieved by axial coordination to the nitrogen of the head group to obtain the immobilized catalyst Rh_2(*S*-DOSP)$_4$-TTDS-Nic-Cellulose (**cel-cat**). A closer depiction of the proposed coordination of the paddlewheel type Rh_2(*S*-DOSP)$_4$ catalyst to the head group of **mod-cel-3** is shown in Fig. 7.

Characterization of the materials

Employing scanning electron microscopy, the microscopic structure of the unmodified cellulose (**cel** (A)), the modified celluloses (**mod-cel-2** (B) / **mod-cel-3** (C)) and the final immobilized catalyst (**cel-cat** (D)) are analyzed and compared. Figure 8 shows that there is almost no change in the morphology between the samples. This result is underlined by analyses of the DNP enhanced ^{1}H→^{13}C CP MAS NMR data of **mod-cel-1**, **mod-cel-2** and **mod-cel-3a** which suggest no significant changes of structural order during the modification of the cellulose (spectra are shown in the supporting information Fig. S5). Furthermore, the separation characteristics of the cellulose by filtration or centrifugation did not change during the modification process. This allows the separation of the immobilized catalyst from reaction mixtures in a similar way compared to cellulose.

After immobilization of Fmoc-TTDS (**3**) on the cellulose material, leading to **mod-cel-1**, the degree of functionalization (DF) is quantitatively analyzed by UV/Vis spectrometry. Here, the amount of the dibenzofulvene-piperidine-adduct which is formed during cleavage of the protecting group from the amino group of the linker on the cellulose using piperidine in DMF, is quantified. With complete deprotection of the amino groups, which can be assumed under the present reaction conditions (Greene and Wuts 2007), the DF of the primary hydroxy groups of the cellulose is determined to be 6.8%. This DF is expected to remain constant, since the reaction conditions in the next step, the attachment of the linker head, are the same as in the attachment of the linker itself.

Since the surface of the material and therefore the obtained degree of functionalization is low compared to the bulk of the cellulose material, the identification of functional groups is a challenging task that requires specific analytical techniques. Here, DNP enhanced ^{1}H→^{13}C CP MAS NMR is employed to identify modifications of the cellulose at the molecular level. Figure 9 shows the comparison of the DNP enhanced ^{1}H→^{13}C CP MAS NMR of cellulose modified with the TTDS linker containing different chemical modifications as they occur during the synthesis steps. For the Fmoc protected TTDS linker grafted on cellulose (**mod-cel-1**, Fig. 9a), characteristic signals at 120–130 ppm as well as at 135–145 ppm referring to aromatic carbons of the Fmoc protection group and a signal at 155 ppm referring to the carbamate carbon of the protecting group are obtained. These signals vanish after the deprotection step (Fig. 9b), indicating the successful Fmoc protection and deprotection of the TTDS linker. On the other hand, the signals at 165–175 ppm which can be assigned to carbon 1 in the ester group and carbon 4 in the amide group do not vanish after deprotection. This observation confirms qualitatively the stable binding of the TTDS linker on the cellulose as well as the stability of the linker itself under the conditions of the deprotection.

After the binding of the nicotinic acid derived linker head (**mod-cel-3a**, Fig. 9c), several signals in the range between 115 and 160 ppm appear that are clearly attributed to aromatic carbons originating from the nicotinic acid derived head group. More importantly a signal at 156 ppm appears which is clearly assigned to the carbon in amide groups, indicating the successful binding of the head group to the linker. Again, after this modification step the signals at 170–175 ppm are preserved which proves the intactness of the linker and its binding to the cellulose after the modification step.

After coupling of the nicotinic acid derived linker head, the degree of functionalization is determined on **mod-cel-3a** as model system for **mod-cel-3** by quantitative ^{19}F NMR according to the procedures described by some of the authors earlier (Li et al. 2020; Liu et al. 2017). Comparing the integrals of the ^{19}F signal of the fluorinated linker derivative at -127 ppm and

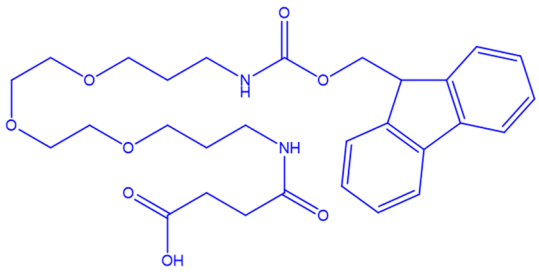

Fmoc-TTDS
3

+

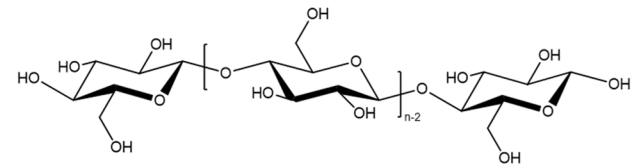

unmodified cellulose
cel

2) EDC•HCl
DMAP

1) $NaOH_{(aq.)}$ / RT, 24 h
2) DMF / RT, 24 h

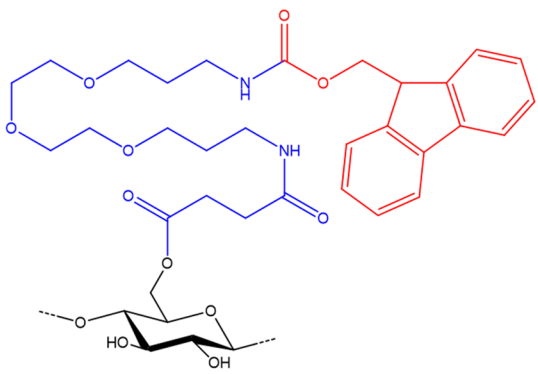

Fmoc-TTDS-Cellulose (87 % @ 6.8 % DF)
mod-cel-1

20 % piperidine

RT, seconds

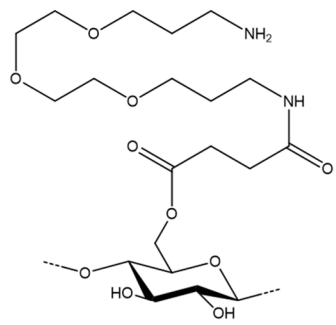

TTDS-Cellulose (94 %)
mod-cel-2

EDC•HCl
DMAP
(4-fluoro)-
nicotinic acid

DMF
RT, 24 h

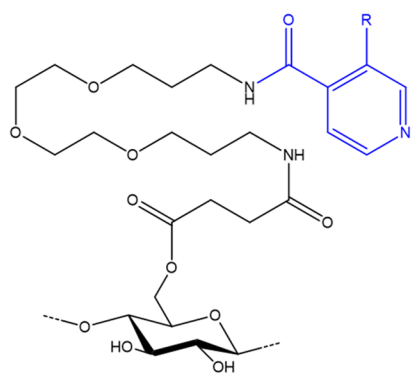

TTDS-Nic-Cellulose
R = H: **mod-cel-3** (87 % @ 6.8 % DF)
R = F: **mod-cel-3a** (84 % @ 6.8 % DF)

120 °C, 8 h, toluene

Rh_2(*S*-DOSP)$_4$

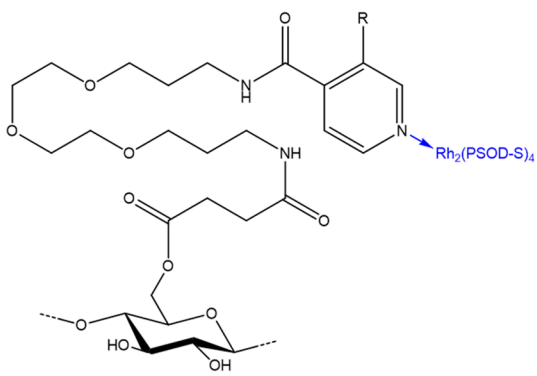

Rh_2(S-DOSP)$_4$-TTDS-Nic-Cellulose (78 % @ 6.8 % DF)
cel-cat

◂**Scheme 3** Immobilization steps of Rh_2(*S*-DOSP)$_4$ on Cellulose. The functionalized derivatives of cellulose are depicted as a modified monosaccharide fragment of the respective polymer

the signal of the barium fluoride reference at -14 ppm (see ESI for detailed calculation) leads to a loading of 0.5 mmol/g of the fluorine labeled linker head with respect to the weight of the material or a degree of functionalization with respect to the primary hydroxy groups of the cellulose of 9.7% (see ESI for detailed calculation). This value is higher than the DF of primary hydroxy groups obtained after immobilization of Fmoc-TTDS and deprotection (6.8%, see above). It can therefore be assumed, that the linker head not only attaches to the linker via amide bond formation, but also to the primary hydroxy groups of the cellulose itself forming ester-bonds. In the final step, the Rh_2(*S*-DOSP)$_4$ is coordinated to the **mod-cel-3** material yielding the heterogeneous **cel-cat** catalyst. The amount of rhodium in this sample is determined using TGA analysis. The burning of the sample in an oxygen rich atmosphere at a maximum of 950 °C leaves a residue of 6.6 wt% of rhodium(III)oxide denoting a rhodium content of 5.4 wt%. with respect to the weight of the heterogeneous catalyst. Additionally, ICP-OES analysis has been applied to the sample to determine the rhodium content. Here, a value of 4.4 wt.-% rhodium has been determined as the rhodium content of the immobilized catalyst which is close to the value obtained by TGA taking the error of the TGA analysis into account. With a loading of 0.5 mmol/g of the coordinating linker head in the material, the degree of complexation can be denoted to 72% (see ESI for detailed calculation).

Catalytic activity tests

The catalytic activity and selectivity of the heterogeneous **cel-cat** are tested in the cyclopropanation reaction (Scheme 4) of styrene with methyl(*E*)-2-diazo-4-phenylbut-3-enoate (**4**) in pentane as solvent. The identity of the products of the cyclopropanation is confirmed by mass spectroscopy. To evaluate the quality of the catalytic activity and selectivity of the **cel-cat** catalyst, it is compared to the analogous homogeneous Rh_2(*S*-DOSP)$_4$ and Rh_2(*R*-DOSP)$_4$ catalysts for which catalytic tests were performed at − 78 °C to obtain good enantioselectivity. Since the activity of the heterogeneous **cel-cat** is assumed to be lower compared to the homogenous ones, the catalytic tests on **cel-cat** are performed at different temperatures up to 35 °C where still no significant loss of enantioselectivity for **cel-cat** is expected.

The identification of the products is performed by comparing the HPLC chromatograms of the known products of the cyclopropanation using the homogeneous Rh_2(*S*-DOSP)$_4$ and Rh_2(*R*-DOSP)$_4$ with the chromatograms of the products using the heterogeneous **cel-cat** catalyst. Since the enantiomeric excess of **d1** produced by the homogeneous Rh_2(*S*-DOSP)$_4$ is known, and additionally, the ratio of **d1** to **ent-d1** is reciprocal in the reaction of Rh_2(*R*-DOSP)$_4$, the peaks of **d1** and **ent-d1** can be clearly assigned in the HPLC chromatogram (see ESI Fig. S9 for a sample chromatogram, using a chiral HPLC column). Analogous to the reaction using the homogeneous Rh_2(*S*-DOSP)$_4$ catalyst, the predominant enantiomer that is formed using the heterogeneous **cel-cat** is the (*S,S*)-product **d1.** The enantiomeric excess will be referred to this (*S,S*)-product **d1**. The diastereomers **d2** and **ent-d2** are not found in any of the product mixtures.

As depicted in Fig. 10, an almost constant enantiomeric excess of 85% at 35 °C during the course of the reaction is achieved for the heterogeneous **cel-cat** compared to 98% at − 78 °C reported for the homogeneous Rh_2(*S*-DOSP)$_4$ catalyst (Davies et al. 1996). This clearly shows the excellent catalytic performance at higher temperatures up to 35 °C of **cel-cat** with respect to enantioselectivity.

Even larger enantiomeric excesses can be achieved for **cel-cat** at lower temperatures but with a remarkable decrease in catalytic activity. In Fig. 11, the enantiomeric excess at 24 h of reaction time (red squares) is depicted with the associated turnover at the same time. At a temperature of − 78 °C, the catalytic activity of **cel-cat** is too low to produce enough product in a reasonable time to calculate a reliable enantiomeric excess. In the temperature range between 0 and 35 °C the turnover after 24 h increases from 18 to 92% while the enantiomeric excess decreases by less than 10% from 92% at 0 °C to 85% at 35 °C. These results clearly demonstrate the excellent enantioselectivity in a broad temperature range where an optimum of catalytic activity and selectivity is expected to be reached at a temperature between 10 and 35 °C.

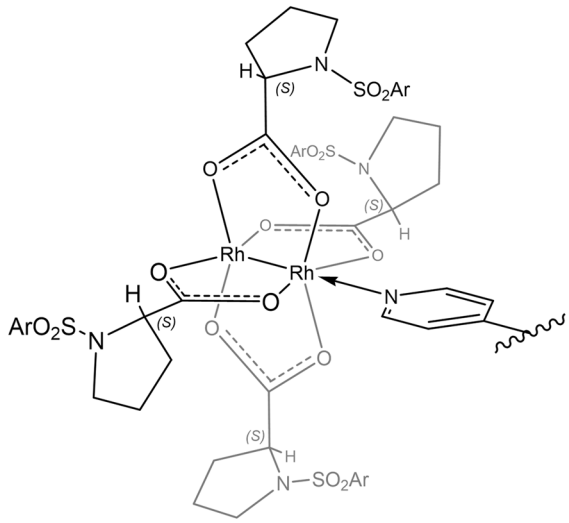

Fig. 7 Spatial representation of the coordination of Rh_2(*S*-DOSP)$_4$ in **cel-cat**

Recyclability and leaching

Finally, the recyclability of the **cel-cat** catalyst as well as its leaching properties are inspected. For the recyclability test, the catalyst is used 4 consecutive times at a temperature of 35 °C, employing recovery, washing, and drying of the catalyst after each cycle.

As shown in Fig. 12, the activity of the catalyst decreases after the first two cycles, and then reaches an almost constant activity in cycle 3 and 4. The selectivity of the catalyst on the other hand, while remaining almost constant during the cycles, rises from cycle 1 to 4. This observation partially coincides with the observation made earlier in the examination of the selectivity and activity at different temperatures. A lower activity of the catalyst also leads to a higher selectivity in these experiments. However, the difference in activity between cycle 3 and 4 is not as prominent as the difference in selectivity, which let us assume that there are more factors involved which influence the behavior of the catalyst. One possible factor is the catalysts mass concentration in the reaction mixture. Due to losses during the recovery process, the mass concentration of the catalyst decreases from the first to the last cycle. This obviously influences the activity but may also have an influence on the selectivity. Further studies to optimize the reaction conditions would be necessary to provide more information on this topic, which is beyond the scope of this work. To analyze the leaching properties, after the first cycle, the supernatant reaction mixture has been analyzed via ICP-OES to reveal the amount of rhodium in the solution used for the catalytic reaction. The ICP-OES (see supporting information Table S2) shows only negligible amounts of rhodium in the reaction mixtures, suggesting a solid bond between the catalyst and the support. These results together with the results from the recyclability test clearly

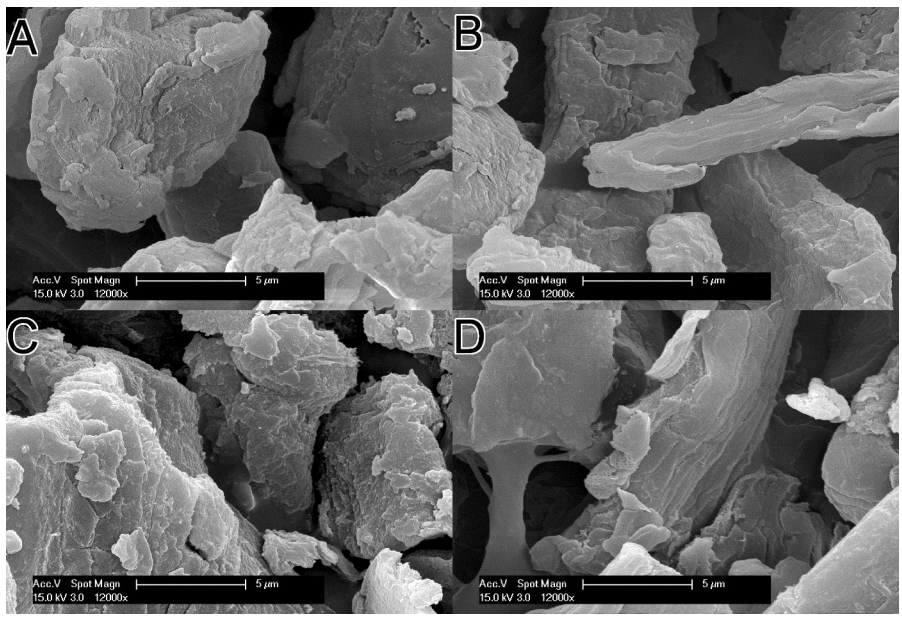

Fig. 8 Comparison of the morphology of **cel** (**a**), **mod-cel-2** (**b**), **mod-cel-3** (**c**) and **cel-cat** (**d**) at 12 000-fold magnification

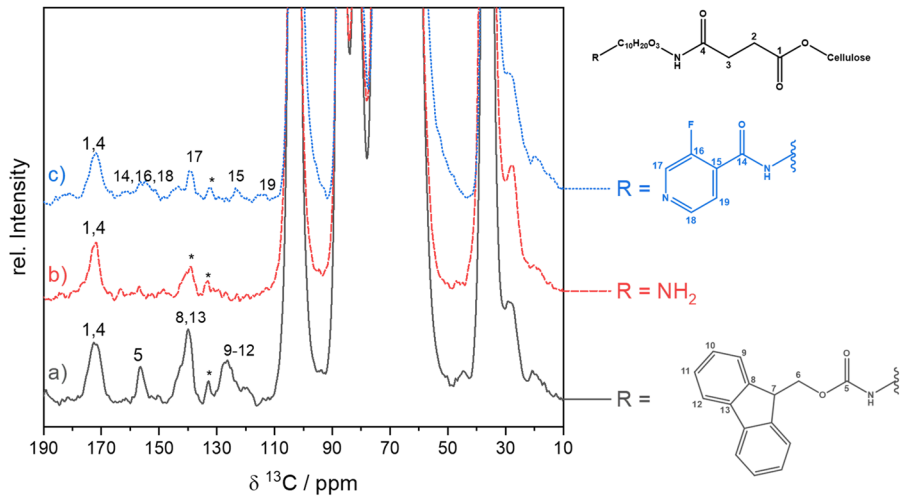

Fig. 9 Comparison of the DNP enhanced $^{1}H \rightarrow {}^{13}C$ CP MAS NMR spectra measured at 10.5 kHz spinning rate of **mod-cel-1** (**a**) (grey/solid line), **mod-cel-2** (**b**) (red/dashed line) and **mod-cel-3a** (**c**) (blue/dotted line). The asterisks indicate the positions of spinning sidebands from the cellulose and radical matrix signals verified by MAS experiments using different spinning rates (see ESI for details)

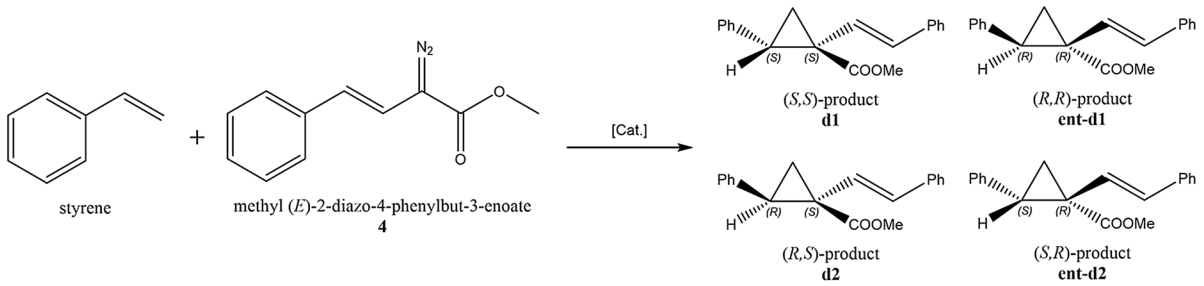

Scheme 4 Cyclopropanation reaction of styrene with methyl(*E*)-2-diazo-4-phenylbut-3-enoate (**4**) to test the catalytic activity of **cel-cat**

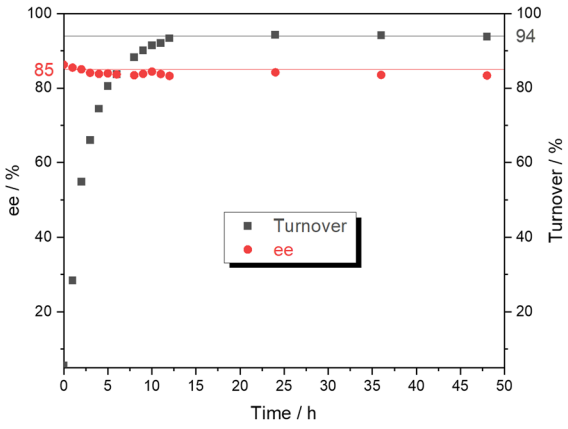

Fig. 10 Evolution of the enantiomeric excess (red/circles) in relation to the turnover of the substrate (grey/squares) in the model cyclopropanation at 35 °C using the heterogeneous **cel-cat** catalyst

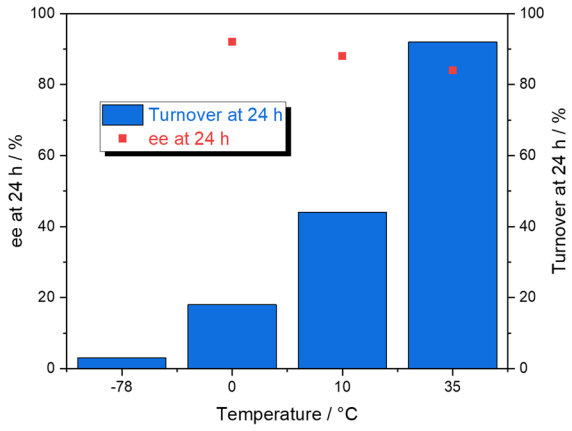

Fig. 11 Enantiomeric excess (red squares) and turnover (blue columns) at different temperatures after a reaction time of 24 h using **cel-cat** in the cyclopropanation reaction of styrene and diazo compound **4**

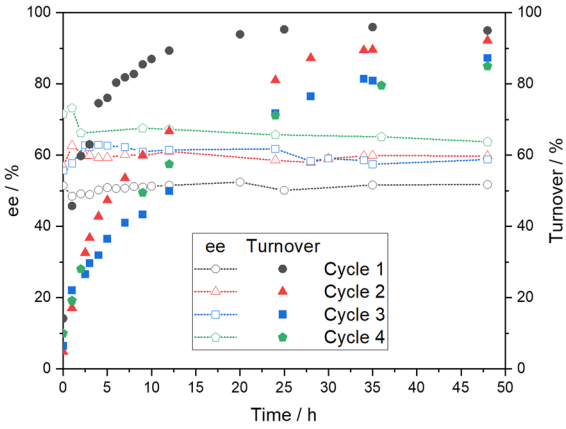

Fig. 12 Comparison of the turnover and ee in the recovery cycles. It has to be noted that the catalyst used in this investigation was obtained from an earlier, non-optimized batch leading to the lower selectivity values

demonstrate the preservation of the heterogeneous catalysts in the cyclopropanation reaction. However, further detailed characterization of the catalyst after each individual cycle in the recycling test has to be performed to investigate changes in the catalyst structure which is beyond the scope of the present work.

Conclusion

A novel cellulose supported heterogeneous catalyst based on the homogeneous Rh_2(*S*-DOSP)$_4$ catalyst has been successfully synthesized and applied in the cyclopropanation reaction of styrene with methyl(*E*)-2-diazo-4-phenylbut-3-enoate (**4**). The synthesis of the enantioselective catalyst has been monitored by DNP enhanced $^{1}H \rightarrow {}^{13}C$ CP MAS NMR, TGA and ICP-OES showing stable coupling of the linker, the coordinating ligand, and the catalyst to cellulose. With UV/Vis, quantitative ^{19}F MAS NMR as well as TGA and ICP-OES, the degree of functionalization and the amount of rhodium have been determined.

The enantiomeric excess produced in the model cyclopropanation reaction has been proven to be excellent for the heterogeneous catalyst with 85% of the (*S*,*S*)-product **d1** at 35 °C. At lower temperatures, even higher enantiomeric excesses of up to 92% have been obtained, however also a significant loss of activity at 0 °C. The recycling experiments showed only minor loss in activity during 4 cycles. Leaching of rhodium species in the catalytic reaction is negligible as stated by ICP-OES results, demonstrating the stability of the heterogeneous catalyst.

The newly formed **cel-cat** catalyst with its versatile linker, opens an easy and sustainable pathway to immobilize different types of dirhodium catalysts to conduct various enantioselective reactions such as cyclopropanations. The length of the linker as well as the coordinating linker head can be easily varied in the synthesis, leaving space for research on chiral catalyst immobilization on biopolymers.

Acknowledgments Financial support by the Deutsche Forschungsgemeinschaft under contract Bu-911/27-1 and HE 3243/4-1 is gratefully acknowledged. The authors acknowledge access to the Jülich-Düsseldorf Biomolecular NMR Center that is jointly run by the Forschungszentrum Jülich and Heinrich-Heine-University Düsseldorf.

Funding Open Access funding enabled and organized by Projekt DEAL.

Declarations

Conflict of interest The authors declare that they have no conflict of interest.

References

Adly FG, Gardiner MG, Ghanem A (2016) Design and synthesis of novel chiral dirhodium(II) carboxylate complexes for asymmetric cyclopropanation reactions. Chemistry (Weinheim an Der Bergstrasse, Germany) 22(10):3447–3461

Adly FG, Ghanem A (2016) Polymer monolith-supported dirhodium(II)-catalyzed continuous flow cyclopropanation in capillary format †. Tetrahedron Lett Tetrahedron Lett 57(8):852–857

Anciaux AJ, Hubert AJ, Noels AF, Petiniot N, Teyssie P (1980) Transition-metal-catalyzed reactions of diazo compounds.

1. Cyclopropanation of double bonds. J. Org. Chem. 45(4):695–702
Awata A, Arai T (2012) Catalytic asymmetric cyclopropanation with diazooxindole. Synlett 24(01):29–32
Berruyer P, Gericke M, Moutzouri P, Jakobi D, Bardet M, Karlson L, Schantz S, Heinze T, Emsley L (2021) Advanced characterization of regioselectively substituted methylcellulose model compounds by DNP enhanced solid-state NMR spectroscopy. Carbohyd Polym 262:117944
Bianchini C, Lee HM (2000) Cyclopropanation of styrene with ethyl diazoacetate catalyzed by chiral and achiral ruthenium 2,6-bis(imino)pyridyl complexes. Organometallics 19(10):1833–1840
Bonnaud B, Cousse H, Mouzin G, Briley M, Stenger A, Fauran F, Couzinier JP (1987) 1-Aryl-2-(aminomethyl)cyclopropanecarboxylic acid derivatives. A new series of potential antidepressants. J Med Chem 30(2):318–325
Boruta DT, Dmitrenko O, Yap GPA, Fox JM (2012) Rh(2)(S-PTTL)(3)TPA-A mixed ligand dirhodium(II) catalyst for enantioselective reactions of α-alkyl-α-diazoesters. Chem Sci 3(5):1589–1593
Cateto CA, Ragauskas A (2011) Amino acid modified cellulose whiskers. RSC Adv 1(9):1695
Chauhan P, Yan N (2015) Nanocrystalline cellulose grafted phthalocyanine: a heterogeneous catalyst for selective aerobic oxidation of alcohols and alkyl arenes at room temperature in a green solvent. RSC Adv 5(47):37517–37520
Chen P-A, Setthakarn K, May JA (2017) A binaphthyl-based scaffold for a chiral dirhodium(II) biscarboxylate ligand with α-quaternary carbon centers. ACS Catal 7(9):6155–6161
Corma A, Garcia H (2006) Silica-bound homogenous catalysts as recoverable and reusable catalysts in organic synthesis. Adv Synth Catal 348(12–13):1391–1412
Davies HML, Antoulinakis EG (2001) Intermolecular metal-catalyzed carbenoid cyclopropanations. In: Organic reactions, pp 1–326
Davies HML, Bruzinski PR, Lake DH, Kong N, Fall MJ (1996) Asymmetric cyclopropanations by rhodium(II) N-(arylsulfonyl)prolinate catalyzed decomposition of vinyldiazomethanes in the presence of alkenes. Practical enantioselective synthesis of the four stereoisomers of 2-phenylcyclopropan-1-amino acid. J Am Chem Soc 118(29):6897–6907
Davies HML, Denton JR (2009) Application of donor/acceptor-carbenoids to the synthesis of natural products. Chem Soc Rev 38(11):3061–3071
Davies HML, Manning JR (2008) Catalytic C–H functionalization by metal carbenoid and nitrenoid insertion. Nature 451(7177):417–424
Davies HML, Morton D (2011) Guiding principles for site selective and stereoselective intermolecular C–H functionalization by donor/acceptor rhodium carbenes. Chem Soc Rev 40(4):1857–1869
Davies HML, Pelphrey PM (2011) Intermolecular C-H Insertions of Carbenoids. In: Organic reactions, pp 75–212
Davies HML, Walji AM (2003) Asymmetric intermolecular C–H activation, using immobilized dirhodium tetrakis((S)-N-(dodecylbenzenesulfonyl)-prolinate) as a recoverable catalyst. Org Lett 5(4):479–482
Davies HML, Walji AM (2005) Universal strategy for the immobilization of chiral dirhodium catalysts. Org Lett 7(14):2941–2944
Davies HML, Walji AM, Nagashima T (2004) Simple strategy for the immobilization of dirhodium tetraprolinate catalysts using a pyridine-linked solid support. J Am Chem Soc 126(13):4271–4280
DeAngelis A, Dmitrenko O, Yap GPA, Fox JM (2009) Chiral crown conformation of Rh(2)(S-PTTL)(4): enantioselective cyclopropanation with alpha-alkyl-alpha-diazoesters. J Am Chem Soc 131(21):7230–7231
Dikarev EV, Kumar DK, Filatov AS, Anan A, Xie Y, Asefa T, Petrukhina MA (2010) Recyclable dirhodium catalysts embedded in nanoporous surface-functionalized organosilica hosts for carbenoid-mediated cyclopropanation reactions. ChemCatChem 2(11):1461–1466
Doyle MP, Bagheri V, Wandless TJ, Harn NK, Brinker DA, Eagle CT, Loh KL (1990) Exceptionally high trans (anti) stereoselectivity in catalytic cyclopropanation reactions. J Am Chem Soc 112(5):1906–1912
Doyle MP, Duffy R, Ratnikov M, Zhou L (2010) Catalytic carbene insertion into C–H bonds. Chem Rev 110(2):704–724
Doyle MP, Hu W (2001) A new enantioselective synthesis of milnacipran and an analogue by catalytic asymmetric cyclopropanation. Adv Synth Catal 343(3):299–302
Doyle MP, Timmons DJ, Tumonis JS, Gau H-M, Blossey EC (2002) Preparation and catalytic properties of immobilized chiral dirhodium(II) carboxamidates. Organometallics 21(9):1747–1749
Doyle MP, Yan M, Gau H-M, Blossey EC (2003) Catalysts with mixed ligands on immobilized supports. Electron Steric Adv Organ Lett 5(4):561–563
Eberhardt AM, Ferreira ML, Damiani DE (2001) Heterogeneization of polymerization catalysts on natural substances. Polym Eng Sci 41(6):946–954
El-Deftar M, Adly G, Gardiner MG, Ghanem A (2012) Chiral dirhodium catalysts: a new era for asymmetric catalysis. COC 16(15):1808–1836
Fung BM, Khitrin AK, Ermolaev K (2000) An improved broadband decoupling sequence for liquid crystals and solids. J Magn Reson (San Diego, Calif.: 1997) 142(1):97–101
Gadakh SK, Dey S, Sudalai A (2015) Rh-catalyzed synthesis of coumarin derivatives from phenolic acetates and acrylates via C–H bond activation. J Org Chem 80(22):11544–11550
Greene TW, Wuts PGM (2007) Greene's protective groups in organic synthesis, 4th edn. Wiley-Interscience, Hoboken, NJ
Groszewicz PB, Mendes P, Kumari B, Lins J, Biesalski M, Gutmann T, Buntkowsky G (2020) N-Hydroxysuccinimide-activated esters as a functionalization agent for amino cellulose: synthesis and solid-state NMR characterization. Cellulose 27(3):1239–1254
Gutmann T, Groszewicz PB, Buntkowsky G (2019) Solid-state NMR of nanocrystals, vol 97. Elsevier, Amsterdam, pp 1–82
Gutmann T, Kumari B, Zhao L, Breitzke H, Schöttner S, Rüttiger C, Gallei M (2017) Dynamic nuclear polarization signal amplification as a sensitive probe for specific

functionalization of complex paper substrates. J Phys Chem C 121(7):3896–3903

Gutmann T, Liu J, Rothermel N, Xu Y, Jaumann E, Werner M, Breitzke H, Sigurdsson ST, Buntkowsky G (2015) Natural abundance 15N NMR by dynamic nuclear polarization: fast analysis of binding sites of a novel amine-carboxyl-linked immobilized dirhodium catalyst. Chemistry (Weinheim an Der Bergstrasse, Germany) 21(9):3798–3805

Höfler MV, Hoinka N, Schäfer T, Horn M, Aussenac F, Fuhrmann-Lieker T, Gutmann T (2021) Light amplification materials based on biopolymers doped with dye molecules—structural insights from 15 N and 13 C solid-state dynamic nuclear polarization. J Phys Chem C 125(39):21550–21558

Huang M-Y, Yang J-M, Zhao Y-T, Zhu S-F (2019) Rhodium-catalyzed Si–H bond insertion reactions using functionalized alkynes as carbene precursors. ACS Catal 9(6):5353–5357

Hultman HM, de Lang M, Nowotny M, Arends IW, Hanefeld U, Sheldon RA, Maschmeyer T (2003) Chiral catalysts confined in porous hosts. J Catal 217(2):264–274

Ibbeson BM, Laraia L, Alza E, O'Connor CJ, Tan YS, Davies HML, McKenzie G, Venkitaraman AR, Spring DR (2014) Diversity-oriented synthesis as a tool for identifying new modulators of mitosis. Nat Commun 5:3155

Keshipour S, Shojaei S, Shaabani A (2013) Palladium nanoparticles supported on ethylenediamine-functionalized cellulose as a novel and efficient catalyst for the Heck and Sonogashira couplings in water. Cellulose 20(2):973–980

Li D, Zhang J, Cai C (2018) Pd nanoparticles supported on cellulose as a catalyst for vanillin conversion in aqueous media. J Org Chem 83(14):7534–7538

Li Z, Davies HML (2010) Enantioselective C–C bond formation by rhodium-catalyzed tandem ylide formation/2,3-sigmatropic rearrangement between donor/acceptor carbenoids and allylic alcohols. J Am Chem Soc 132(1):396–401

Li Z, Rösler L, Herr K, Brodrecht M, Breitzke H, Hofmann K, Limbach H-H, Gutmann T, Buntkowsky G (2020) Dirhodium coordination polymers for asymmetric cyclopropanation of diazooxindoles with olefins: synthesis and spectroscopic analysis. ChemPlusChem 85(8):1737–1746

Li Z, Rösler L, Wissel T, Breitzke H, Gutmann T, Buntkowsky G (2021) Immobilization of a chiral dirhodium catalyst on SBA-15 via click-chemistry: application in the asymmetric cyclopropanation of 3-diazooxindole with aryl alkenes. J CO2 Utilization 52:101682

Li Z, Rösler L, Wissel T, Breitzke H, Hofmann K, Limbach H-H, Gutmann T, Buntkowsky G (2021b) Design and characterization of novel dirhodium coordination polymers—the impact of ligand size on selectivity in asymmetric cyclopropanation. Catal Sci Technol 11(10):3481–3492

Lilly Thankamony AS, Wittmann JJ, Kaushik M, Corzilius B (2017) Dynamic nuclear polarization for sensitivity enhancement in modern solid-state NMR. Prog Nucl Magn Reson Spectrosc 102–103:120–195

Liu J, Fasel C, Braga-Groszewicz P, Rothermel N, Lilly Thankamony AS, Sauer G, Xu Y, Gutmann T, Buntkowsky G (2016) Heterogeneous self-supported dirhodium(ii) catalysts with high catalytic efficiency in cyclopropanation—a structural study. Catal Sci Technol 6(21):7830–7840

Liu J, Groszewicz PB, Wen Q, Thankamony ASL, Zhang B, Kunz U, Sauer G, Xu Y, Gutmann T, Buntkowsky G (2017) Revealing structure reactivity relationships in heterogenized dirhodium catalysts by solid-state NMR techniques. J Phys Chem C 121(32):17409–17416

Liu J, Plog A, Groszewicz P, Zhao L, Xu Y, Breitzke H, Stark A, Hoffmann R, Gutmann T, Zhang K, Buntkowsky G (2015) Design of a heterogeneous catalyst based on cellulose nanocrystals for cyclopropanation: synthesis and solid-state NMR characterization. Chemistry (Weinheim an Der Bergstrasse, Germany) 21(35):12414–12420

Liu J, Xu Y, Groszewicz PB, Brodrecht M, Fasel C, Hofmann K, Tan X, Gutmann T, Buntkowsky G (2018) Novel dirhodium coordination polymers: the impact of side chains on cyclopropanation. Catal Sci Technol 8(20):5190–5200

Maas G (2004) Ruthenium-catalysed carbenoid cyclopropanation reactions with diazo compounds. Chem Soc Rev 33(3):183–190

Miyazawa T, Minami K, Ito M, Anada M, Matsunaga S, Hashimoto S (2016) Enantio-and diastereoselective desymmetrization of α-alkyl-α-diazoesters by dirhodium(II)-catalyzed intramolecular C-H insertion. Tetrahedron 72(27–28):3939–3947

Natori Y, Ito M, Anada M, Nambu H, Hashimoto S (2015) Catalytic asymmetric synthesis of (−)-E-δ-viniferin via an intramolecular C-H insertion of diaryldiazomethane using Rh2(S-TFPTTL)4. Tetrahedron Lett Tetrahedron Lett 56(29):4324–4327

Nickerl G, Stoeck U, Burkhardt U, Senkovska I, Kaskel S (2014) A catalytically active porous coordination polymer based on a dinuclear rhodium paddle-wheel unit. J Mater Chem A 2(1):144–148

Oohara T, Nambu H, Anada M, Takeda K, Hashimoto S (2012) A polymer-supported chiral fluorinated dirhodium(II) complex for asymmetric amination of silyl enol ethers. Adv Synth Catal 354(11–12):2331–2338

Panne P, DeAngelis A, Fox JM (2008) Rh-catalyzed intermolecular cyclopropanation with alpha-alkyl-alpha-diazoesters: catalyst-dependent chemo- and diastereoselectivity. Org Lett 10(14):2987–2989

Perras FA, Luo H, Zhang X, Mosier NS, Pruski M, Abu-Omar MM (2017) Atomic-level structure characterization of biomass pre- and post-lignin treatment by dynamic nuclear polarization-enhanced solid-state NMR. J Phys Chem A 121(3):623–630

Rackl D, Yoo C-J, Jones CW, Davies HML (2017) Synthesis of donor/acceptor-substituted diazo compounds in flow and their application in enantioselective dirhodium-catalyzed cyclopropanation and C–H functionalization. Org Lett 19(12):3055–3058

Rankin AGM, Trébosc J, Pourpoint F, Amoureux J-P, Lafon O (2019) Recent developments in MAS DNP-NMR of materials. Solid State Nucl Magn Reson 101:116–143

Reddy RP, Lee GH, Davies HML (2006) Dirhodium tetracarboxylate derived from adamantylglycine as a chiral catalyst for carbenoid reactions. Org Lett 8(16):3437–3440

Roizen JL, Harvey ME, Du Bois J (2012) Metal-catalyzed nitrogen-atom transfer methods for the oxidation of aliphatic C–H bonds. Acc Chem Res 45(6):911–922

Sauvée C, Rosay M, Casano G, Aussenac F, Weber RT, Ouari O, Tordo P (2013) Highly efficient, water-soluble polarizing agents for dynamic nuclear polarization at high frequency. Angewandte Chemie (Int ed Engl) 52(41):10858–10861

Seyednejhad S, Khalilzadeh MA, Zareyee D, Sadeghifar H, Venditti R (2019) Cellulose nanocrystal supported palladium as a novel recyclable catalyst for Ullmann coupling reactions. Cellulose 26(8):5015–5031

Singh VK, DattaGupta A, Sekar G (1997) Catalytic enantioselective cyclopropanation of olefins using carbenoid chemistry. Synthesis 1997(02):137–149

Sun W, Xia C-G, Wang H-W (2002) Efficient heterogeneous catalysts for the cyclopropanation of olefins. New J Chem 26(6):755–758

Takahashi H, Lee D, Dubois L, Bardet M, Hediger S, de Paëpe G (2012) Rapid natural-abundance 2D 13C–13C correlation spectroscopy using dynamic nuclear polarization enhanced solid-state NMR and matrix-free sample preparation. Angewandte Chemie (Int ed Engl) 51(47):11766–11769

Takeda K, Oohara T, Anada M, Nambu H, Hashimoto S (2010) A polymer-supported chiral dirhodium(II) complex: highly durable and recyclable catalyst for asymmetric intramolecular C-H insertion reactions. Angewandte Chemie (Int ed Engl) 49(39):6979–6983

Takeda K, Oohara T, Shimada N, Nambu H, Hashimoto S (2011) Continuous flow system with a polymer-supported dirhodium(II) catalyst: application to enantioselective carbonyl ylide cycloaddition reactions. Chemistry (Weinheim an Der Bergstrasse, Germany) 17(50):13992–13998

Trindade AF, Coelho JAS, Afonso CAM, Veiros LF, Gois PMP (2012) Fine tuning of dirhodium(II) complexes: exploring the axial modification. ACS Catal 2(3):370–383

de Vos DE, Dams M, Sels BF, Jacobs PA (2002) Ordered mesoporous and microporous molecular sieves functionalized with transition metal complexes as catalysts for selective organic transformations. Chem Rev 102(10):3615–3640

Williams K, Lee E (1985) Importance of drug enantiomers in clinical pharmacology. Drugs 30(4):333–354

Yamada T, Teranishi W, Park K, Jiang J, Tachikawa T, Furusato S, Sajiki H (2020) Development of carbon-neutral cellulose-supported heterogeneous palladium catalysts for chemoselective hydrogenation. ChemCatChem 12(16):4052–4058

Yasukawa T, Miyamura H, Kobayashi S (2015) Cellulose-supported chiral rhodium nanoparticles as sustainable heterogeneous catalysts for asymmetric carbon-carbon bond-forming reactions. Chem Sci 6(11):6224–6229

Yasukawa T, Miyamura H, Kobayashi S (2020) Chiral rhodium nanoparticle-catalyzed asymmetric arylation reactions. Acc Chem Res 53(12):2950–2963

Zhao L, Li W, Plog A, Xu Y, Buntkowsky G, Gutmann T, Zhang K (2014) Multi-responsive cellulose nanocrystal-rhodamine conjugates: an advanced structure study by solid-state dynamic nuclear polarization (DNP) NMR. Phys Chem Chem Phys 16(47):26322–26329

Zhao XS, Bao XY, Guo W, Lee FY (2006) Immobilizing catalysts on porous materials. Mater Today 9(3):32–39

Zhao ZG, Im JS, Lam KS, Lake DF (1999) Site-specific modification of a single-chain antibody using a novel glyoxylyl-based labeling reagent. Bioconjug Chem 10(3):424–430

Zhu B, Liu G, Chen L, Qiu L, Chen L, Zhang J, Zhang L, Barboiu M, Si R, Su C-Y (2016) Metal–organic aerogels based on dinuclear rhodium paddle-wheel units: design, synthesis and catalysis. Inorg Chem Front 3(5):702–710